

# Changes in atomic and electronic structures of amorphous $\text{WO}_3$ films due to electrochemical ion insertion

T. Nanba\*, M. Ishikawa, Y. Sakai, Y. Miura

*Department of Environmental Chemistry and Materials, Okayama University, 3-1-1 Tsushima-Naka, Okayama 700-8530, Japan*

## Abstract

The structural changes in amorphous  $\text{WO}_3$  films were investigated both on the atomic and electronic levels, and the experimental findings were interpreted using molecular orbital calculations. Electrochemical fast intercalation resulted in the splitting of a peak in the valence band region of the X-ray photoelectron spectrum. This splitting could be attributed to the formation of non-bridging oxygen. Decomposition of  $\text{WO}_6$  units into  $\text{WO}_4$  units could also be inferred from the data. This decomposition was, however, not responsible for the split of the photoelectron peak. From the population analyses it was found that the average bond strength decreased due to the intercalation, while select W–O bonds increased in strength. It was expected that these changes in the chemical bonding character lead to localization of electrons and distortion of  $\text{WO}_6$  units, which was consistent with the theoretical interpretations of electrochromism, the intervalence charge transfer model and the small polaron absorption theory.

© 2003 Elsevier B.V. All rights reserved.

*Keywords:* Tungsten trioxide; Structure; X-ray photoelectron spectroscopy; Molecular orbital calculation

## 1. Introduction

After the first report of Deb [1], amorphous tungsten trioxide (a- $\text{WO}_3$ ) films have been extensively studied because of their reversible electrochromic (EC) property, and the films have been used in various applications, such as smart windows, information display, variable reflectance mirrors, etc. [2]. Thorough reviews by Granqvist [2,3] summarize a large number of reports on this matter. According to the reviews, the EC property of  $\text{WO}_3$  films is affected by surface-morphology and porosity of the films, amount and chemical state of water molecules in the films, W/O atomic ratio, etc. Thus, the EC behavior is closely related to the atomic structures of the films, which in turn depend on the preparation methods and conditions.

A large number of polymorphs are found for  $\text{WO}_3$  [3]. Using X-ray diffraction analysis, Nanba et al. [4] have examined the framework structure of a- $\text{WO}_3$  films prepared by various synthetic methods, including vacuum depositions and sol–gel processes. On the basis of this analysis, the structures of amorphous  $\text{WO}_3$  films were effectively classified into two types, which are

analogous to hexagonal and tetragonal forms of crystalline  $\text{WO}_3$  (denoted as h- $\text{WO}_3$  and t- $\text{WO}_3$ , respectively). The framework of h- $\text{WO}_3$  is constructed by 3-, 4- and 6-membered rings formed by  $\text{WO}_6$  octahedra, while the framework of t- $\text{WO}_3$  is made up with only 4-membered rings.

According to Granqvist [3], intercalation of cations such as  $\text{H}^+$ ,  $\text{Li}^+$  or  $\text{Na}^+$  into  $\text{WO}_3$  leads to intricate structural changes, which are not yet fully understood. For example, in the case of crystalline  $\text{WO}_3$ , changes in the lattice parameters [5–8], phase transformation [9,10] and amorphization [6] are known to occur in conjunction with cation intercalations. On a molecular level, the W–O distance increases and the  $\text{WO}_6$  units become distorted due to the formation of  $\text{W}^{5+}$ , as confirmed by X-ray absorption [11]. On the basis of Raman spectroscopy, it was concluded that W–O–W bonds dissociate to form terminal W=O bonds in  $\text{WO}_3$  films [12,13], and cation intercalation leads to a growth of the Raman bands assigned to  $\text{W}^{5+}$ –O and  $\text{W}^{5+}$ =O bonds [14].

On the other hand, phenomenological changes in the electronic states such as valence of W ions seem to be simple as compared with the changes in atomic structure. Granqvist [2,3] references a number of reports of photoelectron spectroscopy. The interpretation of the experimental observations is, however, quite difficult even

\*Corresponding author. Tel.: +81-86-251-8896; fax: +81-86-251-8910.

E-mail address: [tokuro\\_n@cc.okayama-u.ac.jp](mailto:tokuro_n@cc.okayama-u.ac.jp) (T. Nanba).

using theoretical approaches such as molecular orbital (MO) calculations. In fact, various MO methods have been applied to  $\text{WO}_3$  [2,3]. While electronic states have been successfully elucidated, the changes in atomic structure have never been discussed on the basis of theoretical calculations.

In the present study, a- $\text{WO}_3$  films were prepared by r.f.-magnetron sputtering, and their valence band photoelectron spectra were measured. The changes in the valence band spectra were interpreted by means of MO calculations, where a number of cluster models were constructed from various crystalline tungstates. The changes in the atomic structure were also discussed on the basis of chemical bonding character.

## 2. Experimental and calculating procedures

The films were prepared by r.f.-magnetron sputtering. A metallic tungsten plate with 99.99% purity was used as a target and the sputtering was carried out in mixtures of Ar and  $\text{O}_2$  gases under a total pressure of 0.93 Pa. The films were sputtered onto an indium tin oxide-coated glass substrate at an r.f.-power of 30 W, and the thickness of the films was approximately 300 nm.

An electrochemical insertion of  $\text{Li}^+$  ions was performed using a conventional electrochemical cell; working electrode:  $\text{WO}_3$  film, counter electrode: Pt wire, reference electrode: Ag wire and electrolyte: 1 M  $\text{LiClO}_4$ /propylene carbonate solution. The absolute amount of the injected charge was controlled with a Coulomb-meter. The relative amount of the injected charge,  $x$  in  $\text{Li}_x\text{WO}_3$ , was estimated from the weight of the deposited film and the O/W atomic ratio determined by an inductively coupled plasma measurement.

The valence band spectrum was measured using an X-ray photoelectron spectroscopic apparatus with a monochromatic Al  $K\alpha$  radiation ( $h\nu=1486.6$  eV) as an excitation source. Surface contamination was removed by an  $\text{Ar}^+$  etching for less than 30 s, where the etching time was determined to minimize the distortion of valence band spectrum. Inhomogeneous surface charge was neutralized by the combination of a Ni mesh screen and a low energy flood gun ( $\approx 7$  eV) [15]. The electron binding energy was corrected with a C 1s binding energy of adventitious carbon as a reference (284.6 eV). Some crystalline tungstates were also measured for comparison.

First-principle MO calculations were carried out with the self-consistent-charge discrete-variational X $\alpha$  (SCC-DV-X $\alpha$ ) method [16] using a Hartree–Fock–Slater approximation. Cluster models used in the calculation were constructed on the basis of the crystal structures of various tungstates. The clusters were embedded in Madelung potentials generated by point charges outside the clusters to reduce the termination effects. The atomic orbitals (AOs) used in the calculations are W 1s–6s, O

1s–2p, Li 1s–2p and Na 1s–3d. Chemical bonding character was estimated with the Mulliken population analysis [17]. The theoretical intensity of a photoelectron peak was obtained from AO populations multiplied by photo-ionization cross-sections [18,19], and the X-ray photoelectron spectrum was simulated by assuming a Gaussian lineshape for the photoelectron peaks.

## 3. Results and discussion

### 3.1. XPS valence band spectra

Li ions were intercalated into a- $\text{WO}_3$  films with changing intercalating conditions. XPS valence band spectra are shown in Fig. 1. It is known that sputter-deposited amorphous films have different framework structures according to the sputtering conditions. When the partial pressure ratio,  $\text{Ar}/\text{O}_2$ , was 4/1, the films had the h- $\text{WO}_3$  type framework, and in the case of  $\text{Ar}/\text{O}_2=1/1$ , the t- $\text{WO}_3$  type framework was formed [4]. In Fig. 1, the total amount of Li inserted is fixed at  $x=0.6$ , but the insertion time is different. That is, the same amount of Li is inserted into films by changing the insertion rate. Broad peaks are commonly seen at 2–10 and 18–25 eV regions, and another peak appears at 0 eV in the Li-intercalated films. Furthermore, the 2–10 eV peak changes shape according to the insertion time, and the peak in the film of  $\text{Ar}/\text{O}_2=1/1$  is clearly separated into two components when the insertion time is short at 15 and 30 min. A similar spectral change was also observed when a varying amount of Li was inserted over the same insertion time. These results suggest that fast Li insertion leads to the changes not only in electronic structure but also in atomic structure.

The valence band spectra for the several crystalline tungstates were measured to clarify these structural changes (Fig. 2). Monoclinic- $\text{WO}_3$  shows a similar 2–10 eV peak with the as-deposited and slowly inserted amorphous films.  $\text{R}_2\text{WO}_4$  (R=Li, Na and K) crystals are formed by discrete  $\text{WO}_4$  tetrahedra, and all the oxygen atoms are terminal ones, that is, non-bridging oxygen (NBO). The shape of the 2–10 eV peak of these crystals is quite similar to that of the films with the highest insertion rate.  $\text{Na}_2\text{W}_2\text{O}_7$  crystal consists of tetrahedral  $\text{WO}_4$  and octahedral  $\text{WO}_6$  units, and both units include two NBOs. The peak splitting is clearly recognized in this crystal. The splitting of the 2–10 eV peak is commonly observed in the crystals containing NBOs and  $\text{WO}_4$  units, suggesting that the bond dissociation and/or structural reconstruction, that is,  $\text{WO}_6$  to  $\text{WO}_4$ , occur in the fast insertion films. From the experimental spectra, however, the relative contributions of the bond dissociation and the structural reconstruction to the peak separation cannot be distinguished. Therefore, MO calculations were performed to estimate the

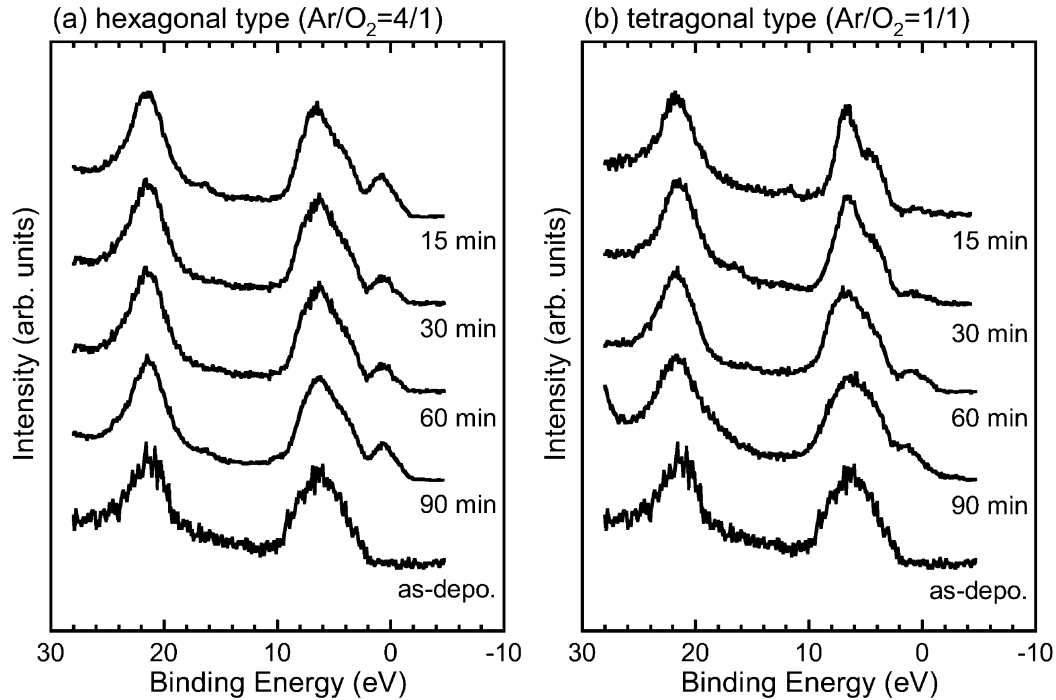


Fig. 1. XPS valence band spectra for the amorphous  $\text{WO}_3$  films with different framework structures, (a) hexagonal and (b) tetragonal type frameworks. The same amount of Li ( $x=0.6$  in  $\text{Li}_x\text{WO}_3$ ) was inserted with changing the insertion time.

contribution of the structural changes to the experimental spectra.

### 3.2. Theoretical interpretation of valence band spectra

The cluster models were constructed from the crystal structures of h- $\text{WO}_3$  [20], t- $\text{WO}_3$  [21],  $\text{Li}_2\text{WO}_4$  [22],

$\text{Na}_2\text{WO}_4$  [23],  $\text{Na}_2\text{W}_2\text{O}_7$  [24] and  $\text{WO}_3 \cdot \text{H}_2\text{O}$  [25]. An example of the cluster model constructed from t- $\text{WO}_3$  is shown in Fig. 3, in which the electronic states of the central  $\text{WO}_6$  unit were evaluated. In the simulation of

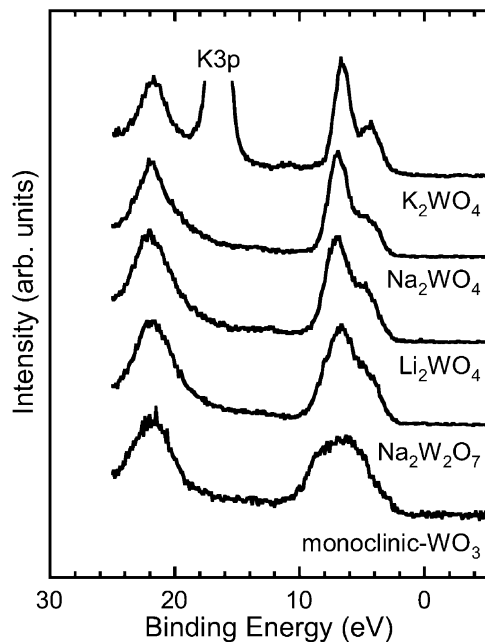


Fig. 2. XPS valence band spectra for the various crystalline tungstates.

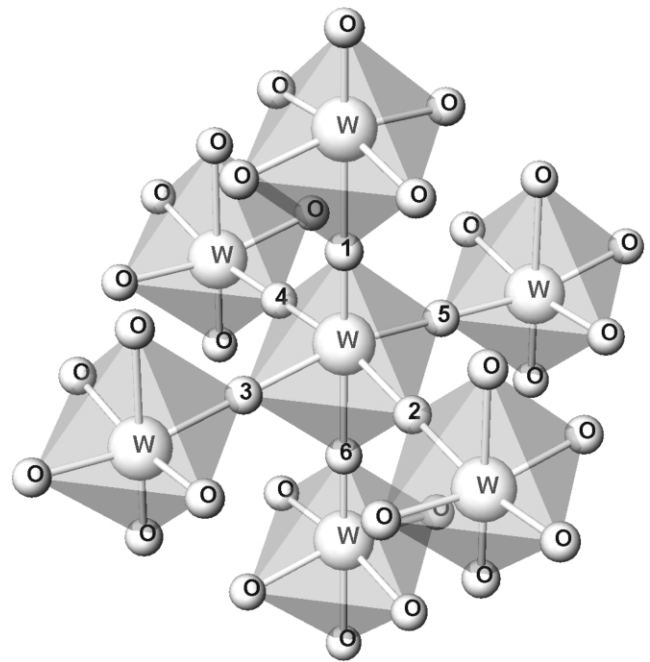


Fig. 3. Cluster model ( $\text{W}_7\text{O}_{36}$ ) constructed from tetragonal  $\text{WO}_3$  crystal [21].

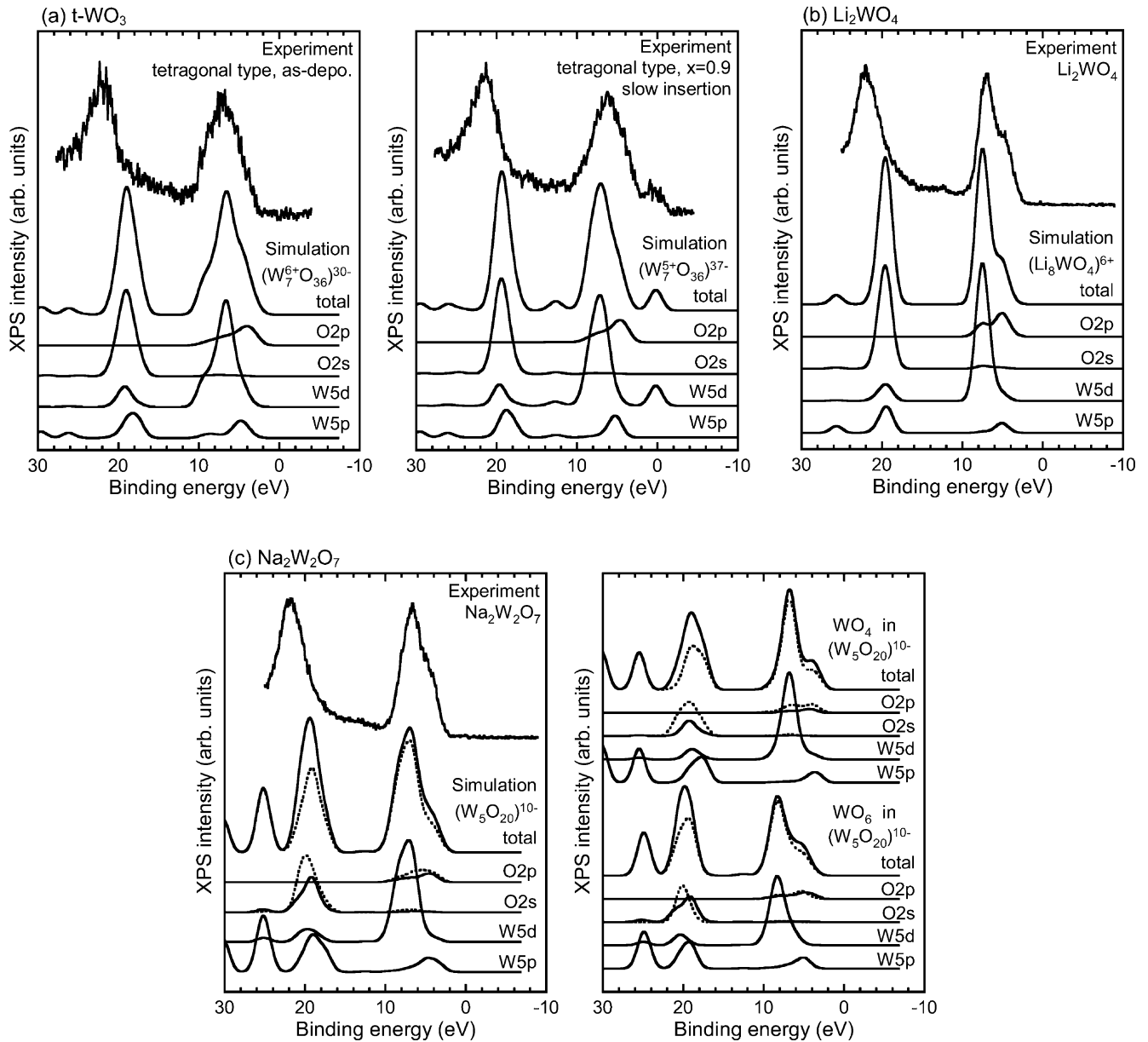


Fig. 4. XPS valence band spectra for the cluster models constructed from (a)  $t\text{-WO}_3$ ; (b)  $\text{Li}_2\text{WO}_4$  and (c)  $\text{Na}_2\text{W}_2\text{O}_7$  crystals. In O 2s and O 2p spectra simulated from  $(\text{W}_5\text{O}_{20})^{10-}$  cluster, the contributions of BO and NBO are drawn by the solid and dotted lines, respectively, and in the total spectra, the dotted lines are obtained by subtracting the contribution of NBO from the solid lines.

XPS valence band spectra, the contribution of bridging oxygens was reduced to half, adjusting the O/W atomic ratio to the actual composition. The simulated valence band spectra are shown in Fig. 4, where the 2–10 eV peak commonly consists of the AOs, W 5p, W 5d and O 2p, with W 5d being the dominant one. The contributions of W 5s and W 6s are negligibly small in the valence band region, and hence their partial spectra are not plotted in Fig. 4. In the density of states (DOS), however, the contribution of W 5d is quite small, and O 2p is the dominant AO. This is due to the large

difference in photo-ionization cross-sections (W 5d:  $6.60 \times 10^3$  barns, O 2p:  $0.24 \times 10^3$  barns) [19].

Fig. 4a shows the valence band spectra obtained from the  $(\text{W}_7\text{O}_{36})$  cluster that is constructed from  $t\text{-WO}_3$  crystal. When the valence of W is 6+ (W  $5d^0$  in conventional notation), the 0 eV peak does not appear in the simulated spectra. In the case of reduced 5+ state (W  $5d^1$ ), however, the 0 eV peak seen in the experimental spectrum is successfully reproduced. It should be noted that the 2–10 eV peak is apparently made up of one component even in the case of  $\text{W}^{5+}$

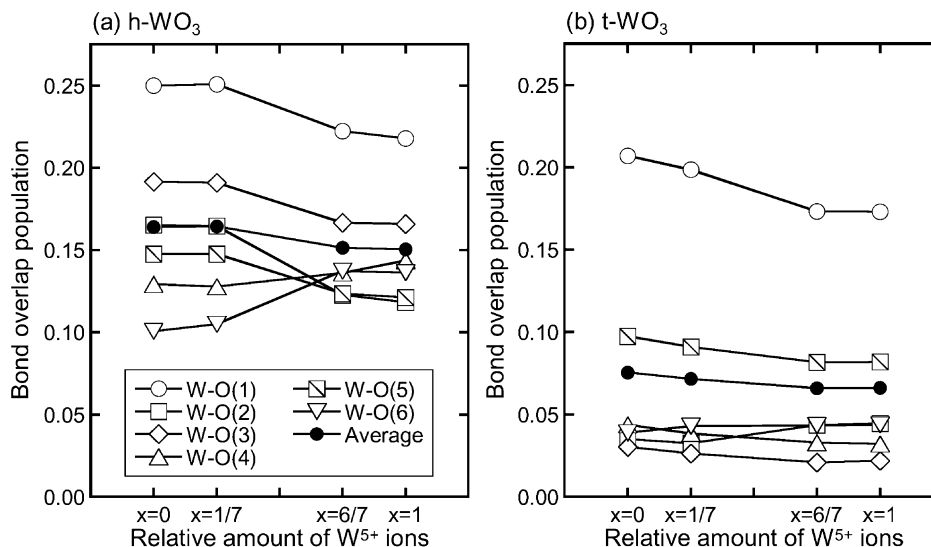


Fig. 5. BOPs for the W–O bonds in the cluster models constructed from (a) h-WO<sub>3</sub> and (b) t-WO<sub>3</sub>.

state, but it is divided into two MO components assigned to W 5d–O 2p and W 5p–O 2p. As for the cluster model constructed from h-WO<sub>3</sub> crystal, almost the same result was obtained. It is therefore surmised that changes in atomic structure other than the change in valence of W are required for the change in shape of the 2–10 eV peak.

Fig. 4b shows the result obtained from the (Li<sub>8</sub>WO<sub>4</sub>)<sup>6+</sup> cluster that is constructed from Li<sub>2</sub>WO<sub>4</sub> crystal. The contribution of Li ions was confirmed in DOS, and in the simulated XPS spectra, however, it was negligibly small so that the AOs of Li ions were not shown in Fig. 4b. The components in the 2–10 eV peak obtained from the WO<sub>4</sub> unit are the same as those from the WO<sub>6</sub> unit in t-WO<sub>3</sub> crystal, but the shape of the peak is, however, clearly separated into two components. The W 5d peak becomes sharper and the W 5p peak becomes smaller as compared to the WO<sub>6</sub> unit. The identical result was observed in the cluster for Na<sub>2</sub>WO<sub>4</sub> crystal. It is therefore concluded that the peak intensity at approximately 5 eV decreases and the 2–10 eV peak splits into two components. It is still not clear which contribution is dominant in the peak separation, the formation of NBO or the change in coordination structure.

Fig. 4c shows the valence band spectra for the (W<sub>5</sub>O<sub>20</sub>)<sup>10-</sup> cluster constructed from Na<sub>2</sub>W<sub>2</sub>O<sub>7</sub> crystal. The results for the WO<sub>6</sub> and WO<sub>4</sub> units are shown separately. The splitting of the 2–10 eV peak is clearly seen both in the WO<sub>6</sub> and WO<sub>4</sub> units. The WO<sub>6</sub> units containing terminal oxygens are also present in WO<sub>3</sub>·H<sub>2</sub>O crystal. The cluster model constructed from WO<sub>3</sub>·H<sub>2</sub>O crystal gave almost the same result as for the WO<sub>6</sub> unit in Na<sub>2</sub>W<sub>2</sub>O<sub>7</sub> crystal. It is concluded from

these results that not the formation of tetrahedral WO<sub>4</sub> units but the formation of NBO is responsible for the peak splitting.

The dissociation of a W–O–W bond produces one terminal W–O bond, and at the same time, the other W loses one oxygen ligand. To the authors' knowledge, fivefold coordinated WO<sub>5</sub> units are not present in crystals, suggesting that the WO<sub>5</sub> unit is unstable. It is therefore surmised that once WO<sub>5</sub> unit is formed, it should turn into WO<sub>4</sub> units. It is consequently concluded that the spectral change in the 2–10 eV region is caused mainly by the formation of NBO and partly by the formation of WO<sub>4</sub> units, and both the structural changes originate from the bond dissociation. It should be noted again that neither the intercalated cations nor W<sup>5+</sup> ions are responsible for the spectral change.

### 3.3. Theoretical interpretation of structural change

Provided that the structural changes originate from the bond dissociation, the question arises why W–O bonds are broken during the fast insertion. It is helpful to examine the change in the chemical bonding character as evaluated from the overlap population analysis. The bond overlap population (BOP) is the number of electrons shared between two atoms, and it is associated with bond order and bond modulus. It is hence assumed that the BOP decreases with introducing ions and electrons preceding the bond dissociation.

Then, in our calculations, electrons were introduced to the (W<sub>7</sub>O<sub>34</sub>) and (W<sub>7</sub>O<sub>36</sub>) cluster models, which have h- and t-WO<sub>3</sub> structures, respectively. In Fig. 5, BOPs for the six W–O bonds in the central WO<sub>6</sub> unit are plotted against the relative amount of W<sup>5+</sup> ions. For

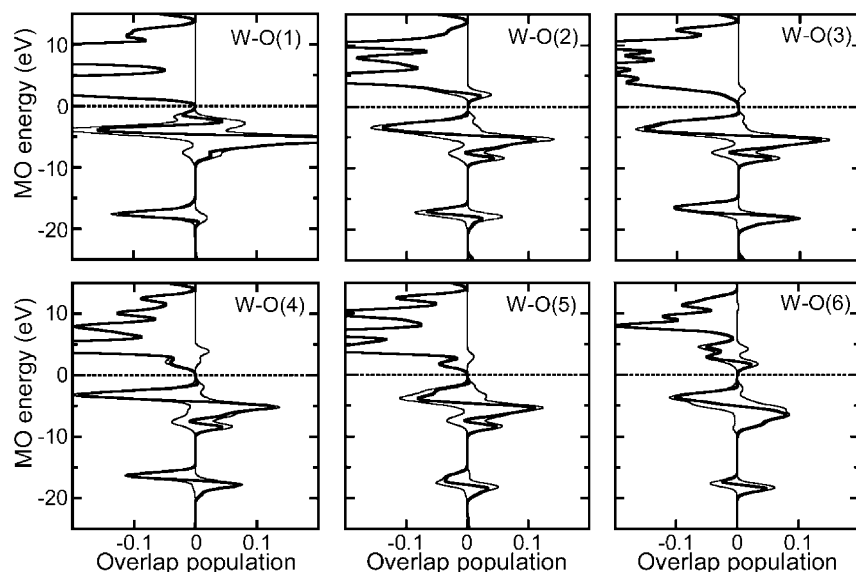


Fig. 6. Overlap population diagrams for the W–O bonds in the cluster model constructed from  $t\text{-WO}_3$ . Numerals in the parentheses indicate the respective oxygen atoms in Figs. 3 and 5. Bonding (positive sign) and anti-bonding (negative sign) overlaps are separately drawn by the thin lines, and the net overlap populations are drawn by the thick lines.

example, when a cluster was doped with one electron, 1 out of 7 W should be reduced to  $5+$ , which is indicated by  $x=1/7$ . Note that with introducing electrons, the BOP decreases for 4 out of 6 bonds, as expected, but it increases for the remaining 2 bonds. This means that not every bond decreases in bond strength due to the electron insertion, or in other words, some W–O bonds lengthen and others shorten. The unequal change in the bond length leads to a distortion of  $\text{WO}_6$  units, creating a so-called small polaron [26]. As is also shown in Fig. 5, the average BOP decreases along with electron doping, resulting in the localization of electrons. This result also supports the intervalence charge transfer model [27].

To understand the surprising change in bonding character, the overlap population diagrams are plotted in Fig. 6, where the HOMO is used as the energy reference (i.e. HOMO=0 eV). When additional electrons are doped, they should be introduced into LUMO levels, that is, bottom of the conduction band. In a conventional notation assuming  $O_h$  symmetry, LUMO is the anti-bonding  $t_{2g}$  orbital that consists of W 5d and O 2p. In W–O(2) and W–O(6) bonds, however, the bottoms of the unoccupied orbitals are in bonding overlap. It is therefore expected that the electrochemical intercalation results in the increase in BOP and the decrease in bond length for these two bonds.

Under moderate intercalating conditions,  $\text{WO}_6$  units are expected to be somewhat distorted but the W–O bonds in these units are not broken, because the reaction must be reversible. However, it was experimentally confirmed that after fast intercalation the films exhibit

poor EC properties. This is probably due to the non-reversible structural changes, such as bond dissociation and decomposition of  $\text{WO}_6$  units into  $\text{WO}_4$  units. In the case of moderate intercalation, the distorted  $\text{WO}_6$  units are relieved into some stable configuration, and under the fast intercalation, however, additional electrons are introduced to the distorted units before the structural relaxation is completed, which finally brings about further deformation and decomposition of the  $\text{WO}_6$  units. Fig. 5 reveals that the hexagonal structure shows much larger BOP than the tetragonal structure, suggesting that the hexagonal structure has higher resistance against the bond dissociation than the tetragonal structure. As shown in Fig. 1, the deformation of the 2–10 eV peak is more significant for the tetragonal structure than that for the hexagonal structure. The difference in the spectral change probably reflects the difference in stability of these structures.

#### 4. Conclusions

Li ions were intercalated into amorphous  $\text{WO}_3$  films prepared by the r.f.-magnetron sputtering method, and the structural change was evaluated by XPS valence band spectra. In the moderate intercalating conditions, no spectral change was observed except for the 0 eV peak. After the vigorous fast insertion, however, the 2–10 eV peak was split into two components. These experimental findings were interpreted on the basis of the MO calculations. According to the simulated spectra, the formation of  $\text{W}^{5+}$  ions brought about the 0 eV peak and had no influence on the 2–10 eV peak. The 2–10

eV peak had contributions from the AOs, W 5p, W 5d and O 2p, where W 5d with its large photo-ionization cross-section was the dominant component in the XPS valence band spectrum. NBO formation was responsible for the deformation of the 2–10 eV peak. It was also indicated that  $\text{WO}_6$  units decomposed into  $\text{WO}_4$  units after the vigorous intercalation. Population analyses were performed to explain the bond dissociation. As expected, the average BOP decreased with electron doping, so that the bond strength of 4 out of 6 W–O bonds in  $\text{WO}_6$  units should decrease and that of the remaining two bonds should increase. These results were consistent with the theoretical interpretations of electrochromism, the intervalence charge transfer model and the small polaron absorption theory.

### Acknowledgments

A part of this work was supported by the Electric Technology Research Foundation of Chugoku. T.N. would like to thank Prof. John Kieffer of the University of Michigan for his helpful comments.

### References

- [1] S.K. Deb, Appl. Opt. Suppl. 3 (1969) 192.
- [2] C.G. Granqvist, Handbook of Inorganic Electrochromic Materials, Elsevier, Amsterdam, 1995.
- [3] C.G. Granqvist, Solar Energy Mater. Solar Cells 60 (2000) 201.
- [4] T. Nanba, T. Takahashi, S. Takano, J. Takada, A. Osaka, Y. Miura, T. Kudo, I. Yasui, J. Ceram. Soc. Jpn. 103 (1995) 222.
- [5] B. Schlasche, R. Schollhorn, Rev. Chim. Mineral 19 (1982) 534.
- [6] M. Figlarz, Proc. Solid State Chem. 19 (1989) 1.
- [7] R.C.T. Slade, B.C. West, G.P. Hall, Solid State Ionics 32–33 (1989) 154.
- [8] J. Oi, A. Kishimoto, T. Kudo, Solid State Ionics 72 (1994) 204.
- [9] Q. Zhong, J.R. Dahn, K. Colbow, Phys. Rev. B 46 (1992) 2554.
- [10] M. Strømme Mattsson, Phys. Rev. B 58 (1998) 11015.
- [11] A. Kuzmin, J. Purans, J. Phys. Cond. Matter 5 (1993) 2333.
- [12] M.F. Daniel, B. Desbat, J.C. Lassegues, R. Garie, J. Solid State Chem. 73 (1988) 127.
- [13] P. Delichere, P. Falaras, M. Froment, A. Hugot-Le Goff, B. Agius, Thin Solid Films 161 (1988) 35.
- [14] S.-H. Lee, H.M. Cheong, C.E. Tracy, A. Mascarenhas, D.K. Benson, S.K. Deb, Electrochim. Acta 44 (1999) 3111.
- [15] S. Matsumoto, T. Nanba, Y. Miura, J. Sur. Sci. Soc. Jpn. 18 (1997) 466, in Japanese.
- [16] H. Adachi, M. Tsukada, C. Satoko, J. Phys. Soc. Jpn. 45 (1978) 875.
- [17] R.S. Mulliken, J. Chem. Phys. 23 (1955) 1833, 1841, 2338, 2343.
- [18] T. Sasaki, H. Adachi, J. Electron Spectrosc. Relat. Phenom. 19 (1980) 261.
- [19] J.J. Yeh, I. Lindau, Atomic Data and Nuclear Data Tables, vol. 32, Academic Press, New York, 1985, p. 1.
- [20] R.W.G. Wyckoff, Crystal Structures, second ed., Wiley, New York, 1964, Chapter VB.
- [21] B. Gerans, G. Nowogrocki, J. Guenot, M. Figlarz, J. Solid State Chem. 29 (1979) 429.
- [22] W.H. Zachariasen, H.A. Plettinger, Acta Cryst. 14 (1961) 229.
- [23] K. Okada, H. Morikawa, F. Marumo, S. Iwai, Acta Cryst. B 30 (1974) 1872.
- [24] K. Okada, H. Morikawa, F. Marumo, S. Iwai, Acta Cryst. B 31 (1975) 1200.
- [25] J.T. Szymanski, A.C. Roberts, Canad. Mineral 22 (1984) 681.
- [26] O.F. Schirmer, V. Wittwer, G. Baur, G. Brandt, J. Electrochem. Soc. 124 (1977) 749.
- [27] B.W. Faughnan, R.S. Crandall, P.M. Heyman, RCA Rev. 36 (1975) 177.